

ScienceAAAS**Type, Density, and Location of Immune Cells Within
Human Colorectal Tumors Predict Clinical Outcome**Jérôme Galon, *et al.**Science* **313**, 1960 (2006);

DOI: 10.1126/science.1129139

**The following resources related to this article are available online at
www.sciencemag.org (this information is current as of December 20, 2008):**

Updated information and services, including high-resolution figures, can be found in the online version of this article at:

<http://www.sciencemag.org/cgi/content/full/313/5795/1960>

Supporting Online Material can be found at:

<http://www.sciencemag.org/cgi/content/full/313/5795/1960/DC1>

A list of selected additional articles on the Science Web sites **related to this article** can be found at:

<http://www.sciencemag.org/cgi/content/full/313/5795/1960#related-content>

This article **cites 29 articles**, 11 of which can be accessed for free:

<http://www.sciencemag.org/cgi/content/full/313/5795/1960#otherarticles>

This article has been **cited by** 147 article(s) on the ISI Web of Science.

This article has been **cited by** 55 articles hosted by HighWire Press; see:

<http://www.sciencemag.org/cgi/content/full/313/5795/1960#otherarticles>

This article appears in the following **subject collections**:

Medicine, Diseases

<http://www.sciencemag.org/cgi/collection/medicine>

Information about obtaining **reprints** of this article or about obtaining **permission to reproduce this article** in whole or in part can be found at:

<http://www.sciencemag.org/about/permissions.dtl>

mantle viscosity and crust thickness) in that region, especially over the Hudson Bay and Scandinavia, two prominent PGR active areas. It is possible that the ICE5G PGR model (13) may underestimate the PGR contribution to GRACE-observed ice mass loss over Greenland. However, the uncertainty of the estimated PGR contribution will not likely account for a significant portion of the -239 ± 23 km³/year ice mass loss observed by GRACE. If we adopt this ICE5G-based PGR contribution of mass rate over Greenland (about -5 km³/year, with uncertainty at 100% of the signal, i.e., ± 5 km³/year), then our GRACE estimate of Greenland ice mass rate is about -234 ± 24 km³/year.

The current GRACE estimate is significantly larger than an earlier estimate (-82 ± 28 km³/year), based on just the first 2 years of data (13). The difference is attributed both to increased melting in the most recent 1.5-year period and to improved filtering and estimation techniques (including use of numerical simulations), and the latter may have played a more important role. Increased recent melting may represent simple interannual variability or accelerated melting driven by steady Arctic warming (20). Despite close agreement between our GRACE estimate and recent radar interferometry estimates (2), quantification of Greenland ice mass balance remains a challenge. For example, another study (21) based on 10 years of radar altimetry data during the period 1992 to 2002 suggests a small mass gain for Greenland ($\sim 11 \pm 3$ km³/year) (2), opposite in sign to the more recent estimate (2). On the other hand, thermomechanical ice models forced by general circulation model climate scenarios predict significant Greenland ice loss in the 21st century (22).

The numerical simulation approach used in this study is useful in interpreting GRACE time-variable gravity fields. It contrasts with the basin kernel function approach (13, 15), in which the focus is on a continent-wide average. Numerical simulations are useful in quantifying spatial leakage of variance and in testing hypotheses concerning possible regional contributors to change, such as the Southeast Glacier or Svalbard. Many error sources may affect our GRACE estimates, which include the remaining GRACE measurement error (after spatial smoothing), uncertainty in the background geophysical models used in GRACE (e.g., the uncorrected ocean pole effect in the release-01 GRACE data and errors in the atmospheric and ocean models over Greenland and surrounding regions), and unquantified other leakage effects.

The conclusion that ice loss has accelerated in recent years is independent of uncertainty in PGR effects, because, regardless of magnitude, PGR should contribute a constant rate to time series of any length. GRACE clearly detects a rate change in the most recent period, suggesting a contribution of about 0.54 mm/year to global sea level rise, well above earlier assessments (23). Time series are still relatively short,

and an understanding of interannual variation in ice mass rates is lacking for Greenland. Without question, the extension of the GRACE mission beyond 2010, or the development of a follow-up mission, will contribute fundamentally to separating contributions of ice mass change from other geophysical signals (such as PGR) that contribute to the observations.

References and Notes

1. W. Krabill *et al.*, *Geophys. Res. Lett.* **31**, L24402 10.1029/2004GL021533 (2004).
2. E. Rignot, P. Kanagaratnam, *Science* **311**, 986 10.1126/science.1121381 (2006).
3. E. Rignot, D. Braaten, S. P. Gogineni, W. B. Krabill, J. R. McConnell, *Geophys. Res. Lett.* **31**, L10401 10.1029/2004GL019474 (2004).
4. B. D. Tapley, S. Bettadpur, M. M. Watkins, C. Reigber, *Geophys. Res. Lett.* **31**, L09607 10.1029/2004GL019920 (2004).
5. Ch. Reigber *et al.*, *J. Geodyn.* **39**, 1 (2005).
6. S. Bettadpur, *Level-2 Gravity Field Product User Handbook*, The GRACE Project (Jet Propulsion Laboratory, Pasadena, CA, 2003).
7. J. Wahr, S. Swenson, V. Zlotnicki, I. Velicogna, *Geophys. Res. Lett.* **31**, L11501 10.1029/2004GL019779 (2004).
8. B. D. Tapley, S. Bettadpur, J. Ries, P. F. Thompson, M. M. Watkins, *Science* **305**, 503 (2004).
9. R. Schmidt *et al.*, *Global Planet. Change* **50**, 112 (2006).
10. D. P. Chambers, J. Wahr, R. S. Nerem, *Geophys. Res. Lett.* **31**, L13310 10.1029/2004GL020461 (2004).
11. J. L. Chen, C. R. Wilson, B. D. Tapley, J. S. Famiglietti, M. Rodell, *J. Geodesy* **79**, 532 10.1007/s00190-005-9 (2005).
12. W. R. Peltier, *Annu. Rev. Earth Planet. Sci.* **32**, 111 10.1146/annurev.earth.32.082503.144359 (2004).
13. I. Velicogna, J. Wahr, *Geophys. Res. Lett.* **32**, L18505 10.1029/2005GL023955 (2005).
14. M. E. Tamisiea, E. W. Leuliette, J. L. Davis, J. X. Mitrovica, *Geophys. Res. Lett.* **32**, L20501 10.1029/2005GL023961 (2005).
15. I. Velicogna, J. Wahr, *Science* 10.1126/science.1123785 (2006).
16. J. L. Chen, B. D. Tapley, C. R. Wilson, *Earth Planet. Sci. Lett.* **248**, 353 (2006).
17. G. Ramillien *et al.*, *Global Planet. Change* **53** (no. 3), 198 (2006).
18. J. L. Chen, C. R. Wilson, K.-W. Seo, *J. Geophys. Res.* **111**, B6, B06408, 10.1029/2005JB004064 (2006).
19. T. Sato *et al.*, *Geophys. J. Inter.* **165**, 729 (2006).
20. F. S. Chapin *et al.*, *Science* **310**, 657 10.1126/science.1117368 (2005).
21. H. J. Zwally *et al.*, *J. Glaciol.* **51**, 509 (2005).
22. P. Huybrechts, J. Gregory, I. Janssens, M. Wilde, *Global Planet. Change* **42**, 83 (2004).
23. J. A. Church *et al.*, in *Climate Change: The Scientific Basis*. Contribution of Working Group 1 to the Third Assessment Report of the Intergovernmental Panel on Climate Change, J. T. Houghton, Ed. (Cambridge Univ. Press, Cambridge, 2001), pp. 639–694.
24. The authors would like to thank the three anonymous reviewers for their insightful comments. This study was supported by the NASA Solid Earth and Natural Hazards and GRACE Program (under grants NNG04G060G, NNG04GP70G, and NNG04GF22G).

Supporting Online Material

www.sciencemag.org/cgi/content/full/1129007/DC1
SOM Text
Fig. S1

20 April 2006; accepted 7 July 2006

Published online 10 August 2006;

10.1126/science.1129007

Include this information when citing this paper.

Type, Density, and Location of Immune Cells Within Human Colorectal Tumors Predict Clinical Outcome

Jérôme Galon,^{1*} Anne Costes,¹ Fatima Sanchez-Cabo,² Amos Kirilovsky,¹ Bernhard Mlecnik,² Christine Lagorce-Pagès,³ Marie Tosolini,¹ Matthieu Camus,¹ Anne Berger,⁴ Philippe Wind,⁴ Franck Zinzindohoué,⁵ Patrick Bruneval,⁶ Paul-Henri Cugnenc,⁵ Zlatko Trajanoski,² Wolf-Herman Fridman,^{1,7} Franck Pagès^{1,7} †

The role of the adaptive immune response in controlling the growth and recurrence of human tumors has been controversial. We characterized the tumor-infiltrating immune cells in large cohorts of human colorectal cancers by gene expression profiling and in situ immunohistochemical staining. Collectively, the immunological data (the type, density, and location of immune cells within the tumor samples) were found to be a better predictor of patient survival than the histopathological methods currently used to stage colorectal cancer. The results were validated in two additional patient populations. These data support the hypothesis that the adaptive immune response influences the behavior of human tumors. In situ analysis of tumor-infiltrating immune cells may therefore be a valuable prognostic tool in the treatment of colorectal cancer and possibly other malignancies.

Tumors in mice and humans often contain infiltrates of immune cells. Experiments with immune-deficient mice have provided data supporting the role of adaptive immunity in cancer immunosurveillance (1–4). Tumor cells can express antigens and become targets for a T cell–mediated adaptive immune response (5, 6). The differentiation of naïve CD4⁺ T cells

into T helper type 1 (T_H1) cells producing interferon gamma (IFN-γ) promotes CD8 T cell–mediated adaptive immunity (7). In mice, immune cells appear to prevent the development of tumors and inhibit tumor progression (1, 3, 4). Anti-tumor immunity also leads to immunoeediting, a process favoring the eventual outgrowth of tumor cells with reduced immunogenicity (3).

The role of immune cells in human neoplasia is less clear (8). Immune cells can release inflammatory mediators with proangiogenic and prometastatic effects (9–14). Tumor-infiltrating lymphocytes in melanoma (15), colorectal cancers (CRCs) (16–18), and ovarian cancers (19, 20) have been shown to inhibit tumor growth and are associated with improved prognoses. After antigen stimulation, a small population of antigen-specific memory T cells remains in the tissues (21). We recently showed that human CRCs with a high density of infiltrating memory and effector memory T cells were less likely to disseminate to lymphovascular and perineural structures and to regional lymph nodes (22). Using the same cohort of patients, we investigated the relationship between the type, density, and location of immune cells within tumors and the clinical outcome of the patients.

To this end, we conducted genomic and in situ immunostaining analyses on tumors from 75 and 415 patients, respectively (table S1). The data were entered into a dedicated Tumoral MicroEnvironment Database (TME.db; access available upon request). We used quantitative real-time polymerase chain reaction to evaluate the expression levels of genes related to inflammation, T_H1 adaptive immunity, and immunosuppression. These genes showed variable expression patterns in the 75 tumors studied (fig. S1). Correlation analyses performed between all genes showed 39 highly significant combinations ($P < 0.0001$) (fig. S1 and table S2). We identified a dominant cluster of co-modulated genes for T_H1 adaptive immunity [genes encoding T-box transcription factor 21, interferon regulatory factor 1, IFN- γ , CD3- ζ , CD8, granulysin, and granzyme B (GZMB)] (Fig. 1A). A hierarchical tree structure classifying the patients according to the expression levels of genes from this cluster revealed an inverse correlation between the expression of these genes and tumor recurrence (P value comparing patient groups, all $P < 0.05$) (Fig. 1B). These data suggest that T_H1 adaptive immunity has a beneficial effect on clinical outcome.

We next used tissue microarrays to investigate the in situ adaptive immune response in the center of the tumor (CT) and the invasive margin (IM) of 415 CRCs. Immunostainings for total T

lymphocytes (CD3), CD8 T cell effectors and their associated cytotoxic molecule (GZMB), and memory T cells (CD45RO) were quantified with the use of a dedicated image analysis workstation (Fig. 2A and figs. S2 to S4). Tumors from patients without recurrence had higher immune cell densities (CD3, CD8, GZMB, and CD45RO) within each tumor region (CT and IM), than did those from patients whose tumors had recurred (Fig. 2B). In each tumor region (CT and IM) and for each marker (CD3, CD8, GZMB, and CD45RO), there was a statistically significant correlation between immune cell density and patient outcome for a large range of cutoff values (fig. S5). In particular, using the cutoff that yielded the minimum P value for disease-free survival, the densities of CD3⁺, CD8⁺, GZMB⁺, and CD45RO⁺ cells in each tumor region (CT and IM) allowed the stratification of patients into groups with different disease-free survival rates [P values corrected after (23), ranging from 1.0×10^{-2} to $4.8 \times$

10^{-6}] and overall survival rates (P values ranging from 5.5×10^{-3} to 7.9×10^{-8}) (Fig. 2C and tables S3 and S4). Reanalyses of the data using 100 repetitions of twofold cross-validations after (24) (tables S3 and S4) or setting the cutoff at the median of the data sets (tables S5 and S6) provided concordant results as to the prognostic value of each immune parameter.

We investigated whether the combined analysis of tumor regions could improve the prediction of patient survival. For all the markers of adaptive immunity (CD3, CD8, GZMB, and CD45RO), the combined analysis of CT plus IM regions [high density in both regions (HiHi) versus low density in both regions (LoLo)] increased the accuracy of prediction of disease-free and overall survival time for the different patient groups, as compared to single-region analysis (Hi versus Lo) (Fig. 2, D to F; figs. S6 and S7; and tables S3 to S6). Data were also analyzed using twofold cross-validation after

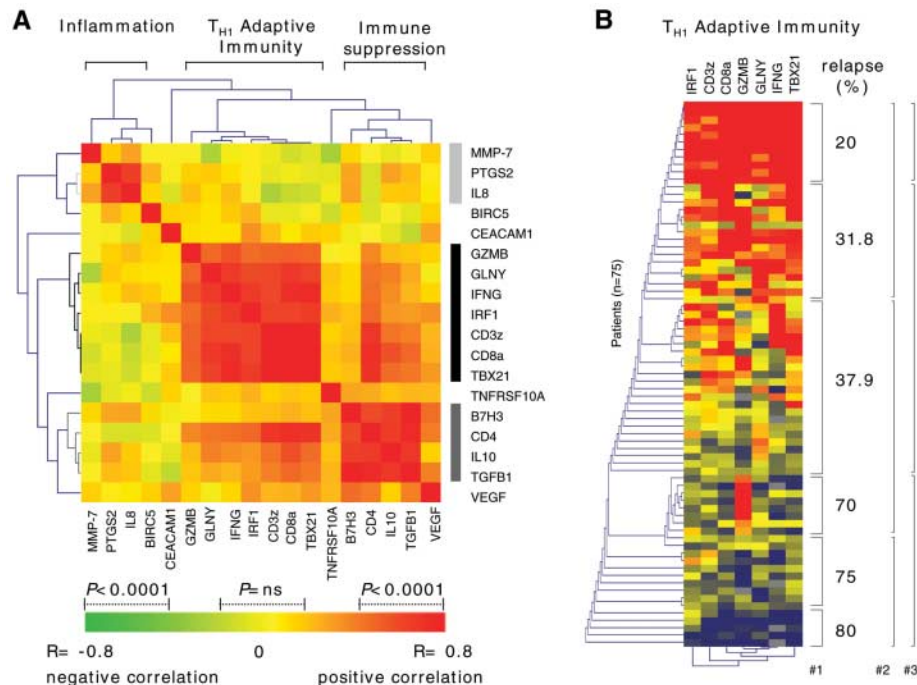


Fig. 1. (A) Correlation analyses performed between the 18 immunogenes were uploaded into the Genesis clustering program (28–30). A correlation matrix followed by unsupervised hierarchical clustering (Pearson uncentered algorithm) is represented from $R = -0.8$ negative correlation (green) to $R = 0.8$ positive correlation (red). For all correlations with $0.4 < R < 0.9$, $P < 0.05$ (table S1). The correlation matrix reveals a dominant cluster of co-modulated genes for T_H1 adaptive immunity and two clusters of genes encoding mediators of inflammation and immunosuppression. (B) Hierarchical tree structure classifying the 75 patients according to the mRNA levels of the seven genes from the T_H1 adaptive cluster, from maximal (red) to minimal (blue) expression levels. The percentage of patients with tumor recurrence (relapse) is indicated. Patients with a homogeneous increased expression of genes for T_H1 adaptive immunity had the best prognosis. Log-rank tests comparing the disease-free survival times between patient groups reached statistical significance ($P < 0.05$ for numbers 1, 2, and 3). In contrast, expression levels of inflammatory and immunosuppressive genes showed no correlation with tumor recurrence. MMP-7, matrix metalloproteinase 7; PTGS2, prostaglandin-endoperoxide synthase 2; IL8, interleukin-8; BIRC5, baculoviral IAP repeat-containing 5 (survivin); CEACAM1, carcinoembryonic antigen-related cell adhesion molecule 1; GLNY, granulysin; IRF1, interferon regulatory factor 1; TBX, T-box 21 (TBET); TNFRSF10A, tumor necrosis factor receptor superfamily, member 10a (TRAILR1); TGFB1, transforming growth factor- β 1; VEGF, vascular endothelial growth factor.

¹INSERM U 255, Paris, 75006 France; Université Paris-Descartes Paris 5, Faculté de Médecine, Paris, 75006 France; and Université Pierre et Marie Curie Paris 6, Institut des Cordeliers, Paris, 75006 France. ²Institute for Genomics and Bioinformatics, Graz University of Technology, Graz, Austria. ³Department of Pathology, ⁴Department of Digestive Surgery, Avicenne Hospital, Bobigny, 93017 France. ⁵Department of General and Digestive Surgery, ⁶Department of Pathology, ⁷Department of Immunology, Georges Pompidou European Hospital, AP-HP, Paris, 75015 France.

*To whom correspondence should be addressed. E-mail: jerome.galon@u255.bhdc.jussieu.fr
 †These authors contributed equally to this work.

(24) (100 repetitions for each marker), showing highly significant differences (tables S3 and S4). $CD3_{CT}/CD3_{IM}$ density was associated with the smallest *P* values for disease-free and overall survival analyses ($P = 7.6 \times 10^{-8}$ and $P = 4.0 \times 10^{-7}$, respectively) (tables S3 and S4). To confirm these results, we analyzed an additional cohort of patients who were different from those in the first series and a third cohort of CRC patients from another hospital. For each cohort, we determined the median cutoff values for $CD3_{CT}/CD3_{IM}$ density (50% of patients with a high density and 50% of patients with a low density). The two independent cohorts (Fig. 2, E and F) confirmed the data

obtained on the first series (Fig. 2D). All statistical analyses were also performed for the subgroup of patients without concomitant distant metastasis [Union Internationale Centre le Cancer–Tumor Node Metastasis (UICC-TNM) cancer stages I, II, and III]. Significant *P* values were observed for $CD3_{CT}/CD3_{IM}$, $CD8_{CT}/CD8_{IM}$, and $CD45RO_{CT}/CD45RO_{IM}$ densities for predicting disease-free survival and overall survival (figs. S8 and S9 and tables S7 to S10).

We determined whether these immune criteria could discriminate patient outcome at each step of cancer progression. Patients were stratified according to the UICC-TNM classification (25) (Fig. 3A). A strong in situ immune reac-

tion in both tumor regions correlated with a favorable prognosis regardless of the local extent of the tumor and of invasion of regional lymph nodes (stages I, II, and III). Conversely, a weak in situ immune reaction in both tumor regions correlated with a poor prognosis even in patients with minimal tumor invasion (stage I) (Fig. 3B). We recently demonstrated the importance of the density of $CD45RO^+$ memory T cells in limiting the tumor dissemination of CRCs (22). We found that patients with low densities of $CD3^+$ cells and $CD45RO^+$ memory T cells in both tumor regions (CT and IM) had a very poor prognosis, similar to that of patients with concomitant distant metastasis

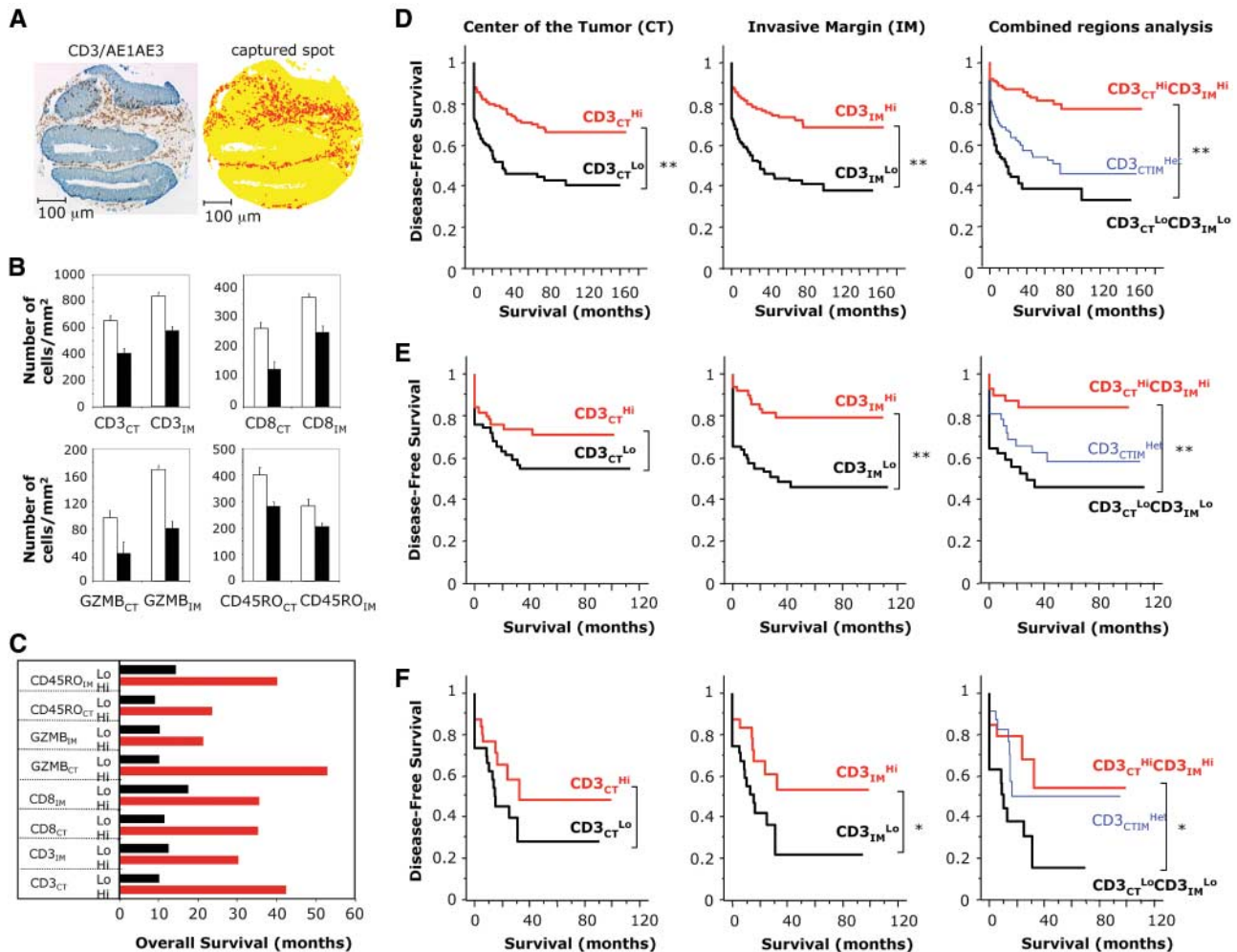


Fig. 2. (A) (Left) A representative example of CD3 immunostaining of a CRC tissue microarray (top). $CD3^+$ T cells (brown) and tumor cells (blue) are shown. (Right) Digital image analyzed with the image software SpotBrowser, with tissue represented in yellow and $CD3^+$ cells represented in red. The densities of adaptive immune cells ($CD3^+$, $CD8^+$, $GZMB^+$, and $CD45RO^+$ cells) were recorded as the number of positive cells per unit of tissue surface area. (B) Comparison of the mean (\pm SE) of immune cell densities in the CT and IM from patients with tumor recurrence (black bars) or without tumor recurrence (white bars). (C) Overall survival time for all patients, accounting for censoring (75th percentile), with high densities (red bars) or low densities (black bars) of adaptive immune cells in each tumor region (CT or IM). (D to F) Three independent cohorts of CRC patients were analyzed in

a blinded manner for $CD3_{CT}/CD3_{IM}$ patterns [(D), $n = 415$; (E), $n = 119$; (F), $n = 69$ patients]. Kaplan-Meier curves illustrate the duration of disease-free survival according to the $CD3^+$ cell density in the CT (left panels) or IM (middle panels) and in both tumor regions (right panels). In each cohort, for each tumor region, high (Hi) and low (Lo) $CD3$ densities were plotted according to the cutoff value of $CD3^+$ cell density defined at the median of the cohort (50% of patients with high cell density and 50% of patients with low cell density). In single-region analysis (left and middle panels), red lines indicate $CD3^{Hi}$ and black lines indicate $CD3^{Lo}$. In combined analysis (right panels), red lines indicate $CD3_{CT}^{Hi}CD3_{IM}^{Hi}$, black lines indicate $CD3_{CT}^{Lo}CD3_{IM}^{Lo}$, and blue lines indicate heterogeneous $CD3$ densities with $CD3_{CT}^{Lo}$ plus $CD3_{IM}^{Hi}$ or $CD3_{CT}^{Hi}$ plus $CD3_{IM}^{Lo}$ ($CD3_{CT/IM}^{Het}$).

(stage IV) (Fig. 3C). In multivariate analysis, after adjusting for tumor invasion (T stage), tumor differentiation, and lymph node invasion (N stage), CD3_{CT}/CD3_{IM} density (HiHi, Heterogeneous, and LoLo) remained an independent

prognostic factor, with the highest hazard ratio (HR) and the smallest *P* value in disease-free survival analysis [HR = 2.379; *P* = 1.4 × 10⁻⁶, corrected after (26)] (table S11). CD3_{CT}/CD3_{IM} density was the only independent parameter

associated with overall survival (HR = 1.89; *P* = 1.2 × 10⁻⁵) (table S12). The histopathological parameters were no longer associated with disease-free and overall survival in patients with coordinated high or low densities of the immune markers in both tumor regions (HiHi versus LoLo) (tables S11 and S12).

Our results suggest that once human CRCs become clinically detectable, the adaptive immune response plays a role in preventing tumor recurrence. Despite immunoeediting (2), the beneficial effect of the adaptive immunity may persist throughout tumor progression (stages II and III). Intratumoral T cells could modify tumor stroma or tumor cells in ways that attenuate the metastatic potential of tumor cells. We found a positive correlation between the presence of markers for T_H1 polarization and of cytotoxic and memory T cells and a low incidence of tumor recurrence. This argues for immune-mediated rejection of persistent tumor cells after surgery. We hypothesize that the trafficking properties and long-lasting anti-tumor capacity of memory T cells (27) play a central role in the control of tumor recurrence.

The type, density, and location of immune cells in CRCs had a prognostic value that was superior to and independent of those of the UICC-TNM classification (25). This suggests that time to recurrence and overall survival time are governed in large part by the state of the local adaptive immune response. The immunological criteria that we have used may lead to revision of the current indicators of clinical outcome and may help identify the high-risk patients who would benefit most from adjuvant therapy. Finally, this approach may be useful for the investigation of other tumor types.

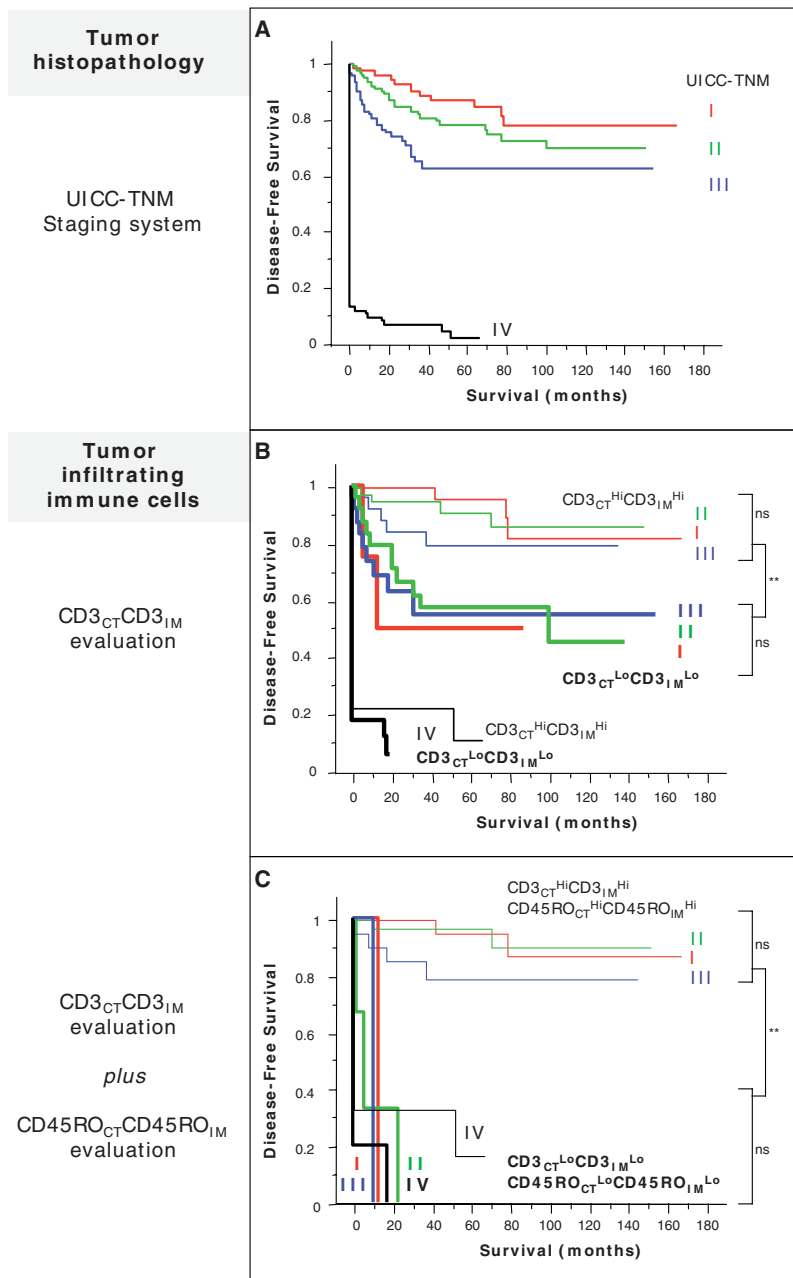


Fig. 3. (A) Kaplan-Meier curves illustrate the duration of disease-free survival according to the UICC-TNM stages [stage I, red line (*n* = 75 patients); stage II, green line (*n* = 137); stage III, blue line (*n* = 99), and stage IV, black line (*n* = 95)] in patients with CRCs. **(B)** Kaplan-Meier curves illustrate the duration of disease-free survival according to the UICC-TNM stages [as in (A)] and according to the density of CD3⁺ cells in combined tumor regions (CD3_{CT}^{Lo}CD3_{IM}^{Lo}, thick lines, *n* = 93 patients; CD3_{CT}^{Hi}CD3_{IM}^{Hi}, thin lines, *n* = 109). The subgroup of patients that did not appear to have a coordinated in situ immune reaction in tumor regions (Hi/Lo or Lo/Hi for CD3⁺ cell densities) presented similar Kaplan-Meier curves as the entire cohort (fig. S10). **(C)** Kaplan-Meier curves illustrate the duration of disease-free survival according to the UICC-TNM stages and to the density of CD3⁺ and CD45RO⁺ cells in combined tumor regions (CD3_{CT}^{Lo}CD3_{IM}^{Lo} plus CD45RO_{CT}^{Lo}CD45RO_{IM}^{Lo}, thick lines, *n* = 16 patients; CD3_{CT}^{Hi}CD3_{IM}^{Hi} plus CD45RO_{CT}^{Hi}CD45RO_{IM}^{Hi}, thin lines, *n* = 88). Cutoff values were 250, 640, 60, and 190 for CD3_{CT}, CD3_{IM}, CD45RO_{CT}, and CD45RO_{IM}, respectively. In (B) and (C), log-rank statistical test, ** *P* < 10⁻⁴; ns, not significant.

References and Notes

- G. P. Dunn, A. T. Bruce, H. Ikeda, L. J. Old, R. D. Schreiber, *Nat. Immunol.* **3**, 991 (2002).
- G. P. Dunn, L. J. Old, R. D. Schreiber, *Annu. Rev. Immunol.* **22**, 329 (2004).
- V. Shankaran *et al.*, *Nature* **410**, 1107 (2001).
- G. Zhou, Z. Lu, J. D. McCadden, H. I. Levitsky, A. L. Marson, *J. Exp. Med.* **200**, 1581 (2004).
- T. Boon, J. C. Cerottini, B. Van den Eynde, P. van der Bruggen, A. Van Pel, *Annu. Rev. Immunol.* **12**, 337 (1994).
- P. van der Bruggen *et al.*, *Science* **254**, 1643 (1991).
- S. J. Szabo, B. M. Sullivan, S. L. Peng, L. H. Glimcher, *Annu. Rev. Immunol.* **21**, 713 (2003).
- K. E. de Visser, A. Eichten, L. M. Coussens, *Nat. Rev. Cancer* **6**, 24 (2006).
- L. M. Coussens, Z. Werb, *Nature* **420**, 860 (2002).
- F. R. Greten *et al.*, *Cell* **118**, 285 (2004).
- D. Pardoll, *Nature* **411**, 1010 (2001).
- D. Pardoll, *Annu. Rev. Immunol.* **21**, 807 (2003).
- E. Pikarsky *et al.*, *Nature* **431**, 461 (2004).
- J. W. Pollard, *Nat. Rev. Cancer* **4**, 71 (2004).
- C. G. Clemente *et al.*, *Cancer* **77**, 1303 (1996).
- P. K. Baier *et al.*, *Tumour Biol.* **19**, 205 (1998).
- A. C. Diederichsen, J. B. Hjelmberg, P. B. Christensen, J. Zeuthen, C. Fenger, *Cancer Immunol. Immunother.* **52**, 423 (2003).
- Y. Naito *et al.*, *Cancer Res.* **58**, 3491 (1998).
- E. Sato *et al.*, *Proc. Natl. Acad. Sci. U.S.A.* **102**, 18538 (2005).
- L. Zhang *et al.*, *N. Engl. J. Med.* **348**, 203 (2003).

21. F. Sallusto, J. Geginat, A. Lanzavecchia, *Annu. Rev. Immunol.* **22**, 745 (2004).
22. F. Pages *et al.*, *N. Engl. J. Med.* **353**, 2654 (2005).
23. D. G. Altman, B. Lausen, W. Sauerbrei, M. Schumacher, *J. Natl. Cancer Inst.* **86**, 829 (1994).
24. D. Faraggi, R. Simon, *Stat. Med.* **15**, 2203 (1996).
25. L. Sobin, C. Wittekind, *TNM Classification of Malignant Tumors* (Wiley-Liss, ed. 6, New York, 2002).
26. N. Hollander, W. Sauerbrei, M. Schumacher, *Stat. Med.* **23**, 1701 (2004).
27. R. Xiang, H. N. Lode, S. D. Gillies, R. A. Reisfeld, *J. Immunol.* **163**, 3676 (1999).
28. J. Galon *et al.*, *FASEB J.* **16**, 61 (2002).
29. F. Pages *et al.*, *Blood* **105**, 1632 (2005).
30. A. Sturn, J. Quackenbush, Z. Trajanoski, *Bioinformatics* **18**, 207 (2002).
31. We thank A. Rodi and M. Pelegrin for expert technical assistance; I. Gresser for helpful comments and critical review of the manuscript; and D. Frucht, C. Anderson, and T. Pokrovskaya for critically reading the manuscript. Supported by the Association pour la Recherche sur le Cancer (ARC) through the Alliance pour la Recherche sur le Cancer network (ARECA), INSERM, Action Concertée Incitative ACI IMPBio, Université Paris-

Descartes Paris 5, and the Austrian Federal Ministry of Education, Science and Culture (GBN-AU project Bioinformatics Integration Network).

Supporting Online Material

www.sciencemag.org/cgi/content/full/313/5795/1960/DC1
Materials and Methods
Figs. S1 to S10
Tables S1 to S12

25 April 2006; accepted 30 August 2006
10.1126/science.1129139

Volatile Chemical Cues Guide Host Location and Host Selection by Parasitic Plants

Justin B. Runyon, Mark C. Mescher, Consuelo M. De Moraes*

The importance of plant volatiles in mediating interactions between plant species is much debated. Here, we demonstrate that the parasitic plant *Cuscuta pentagona* (dodder) uses volatile cues for host location. *Cuscuta pentagona* seedlings exhibit directed growth toward nearby tomato plants (*Lycopersicon esculentum*) and toward extracted tomato-plant volatiles presented in the absence of other cues. Impatiens (*Impatiens wallerana*) and wheat plants (*Triticum aestivum*) also elicit directed growth. Moreover, seedlings can distinguish tomato and wheat volatiles and preferentially grow toward the former. Several individual compounds from tomato and wheat elicit directed growth by *C. pentagona*, whereas one compound from wheat is repellent. These findings provide compelling evidence that volatiles mediate important ecological interactions among plant species.

Plant volatiles serve as important foraging cues for both insect herbivores and their natural enemies and can convey complex information regarding plant location, identity, and condition (1–5). It has been suggested that volatiles may have similar importance for interactions among plants, but such claims have remained controversial (6–13) and where plant-plant volatile effects have been demonstrated, their ecological importance remains unclear (6–9). Previous work on volatile-mediated interactions among plant species has dealt with the role of volatiles induced by herbivory or other environmental stressors in initiating defensive responses in neighboring plants (7, 14–19). Parasitic plants, which to survive must rapidly locate and attach to other plants, provide an alternative system in which host-plant volatiles might be expected to play an important role.

Parasitic plants are important components of both natural and agricultural ecosystems and have considerable influence on the structure and dynamics of the communities they inhabit (20, 21). Yet, little is known about the ecology of interactions between parasitic plants and their hosts. Like insect herbivores, para-

sitic plants exhibit various “foraging” patterns (22–25) and are capable of “selecting” among potential hosts (22–25), but the mechanisms involved in host location and discrimination are not well understood.

Flowering plants in the genus *Cuscuta* are obligate parasites with little photosynthetic capability; they obtain nutrients by attaching to aboveground shoots of other plants (26) (Fig. 1). *Cuscuta* spp. are important agricultural pests, included on the U.S. Department

of Agriculture’s *Top Ten Weeds List*, and can be difficult to control without also impacting host plants (27). Seeds of *Cuscuta* spp. contain minimal energy reserves, allowing growth of only several centimeters, and upon germination, the rootless seedlings must locate and attach to a suitable host within a few days (26). In some parasitic plants, contact with chemical cues secreted from host-plant roots is required for germination (28, 29), but *Cuscuta* spp. have no specialized germination requirements and must depend on seedling “foraging” for host-plant location (26) (fig. S1). After germination, *C. pentagona* seedlings exhibit a rotational growth habit (circumnutation) until contacting a host (26) (movie S1). Host secondary metabolites are known to influence the belowground growth of parasitic plants that attach to host roots (28, 29), and host-derived chemicals also induce haustorial development by these parasites (30). However, the role of host-derived compounds in aboveground host location by *Cuscuta* spp. has not previously been determined.

In this study, we explored host finding by seedlings of *C. pentagona*. First, we examined whether *C. pentagona* seedlings exhibit directed growth toward host plants (potted 20-day-old tomato seedlings). The basal end of a *C. pentagona* seedling was inserted into a water vial placed at the center of a dry filter-

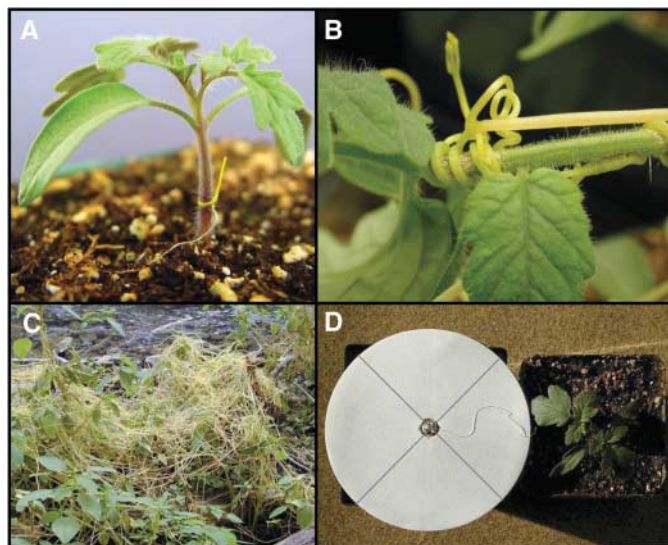


Fig. 1. Parasitic plants in the genus *Cuscuta*. (A) *C. pentagona* seedling attaching to a tomato plant. (B) Vines of *C. pentagona* coiled around the petiole of a tomato leaf. (C) Growth habit of *Cuscuta*. (D) *C. pentagona* seedling growing toward a tomato plant across a filter-paper disc.

Department of Entomology, Pennsylvania State University, University Park, PA 16802, USA.

*To whom correspondence should be addressed. E-mail: czd10@psu.edu